

# THE ALU<sup>+</sup> CONCEPT: N-TYPE SILICON SOLAR CELLS WITH SURFACE-PASSIVATED SCREEN-PRINTED ALUMINUM-ALLOYED REAR EMITTER

Robert Bock<sup>1</sup>, Jan Schmidt<sup>1</sup>, Susanne Mau<sup>1</sup>, Bram Hoex<sup>2</sup>, Erwin Kessels<sup>2</sup>, and Rolf Brendel<sup>1</sup>

<sup>1</sup>Institut für Solarenergieforschung Hameln (ISFH), Am Ohrberg 1, D-31860 Emmerthal, Germany

<sup>2</sup>Dep. of Applied Physics, Eindhoven University of Technology, 5600 MB Eindhoven, The Netherlands

## ABSTRACT

Aluminum-doped  $p$ -type (Al- $p^+$ ) silicon emitters fabricated by means of screen-printing and firing are effectively passivated by plasma-enhanced chemical-vapor deposited (PECVD) amorphous silicon (a-Si) and atomic-layer-deposited (ALD) aluminum oxide (Al<sub>2</sub>O<sub>3</sub>) as well as Al<sub>2</sub>O<sub>3</sub>/SiN<sub>x</sub> stacks, where the silicon nitride (SiN<sub>x</sub>) layer is deposited by PECVD. While the a-Si passivation of the Al- $p^+$  emitter results in an emitter saturation current density  $J_{0e}$  of 246 fA/cm<sup>2</sup>, the Al<sub>2</sub>O<sub>3</sub>/SiN<sub>x</sub> double layers result in emitter saturation current densities as low as 160 fA/cm<sup>2</sup>, which is the lowest  $J_{0e}$  reported so far for screen-printed Al-doped  $p^+$  emitters. Moreover, the Al<sub>2</sub>O<sub>3</sub> as well as the Al<sub>2</sub>O<sub>3</sub>/SiN<sub>x</sub> stacks show an excellent stability during firing in a conveyor belt furnace at 900°C. We implement our newly developed passivated Al- $p^+$  emitter into an  $n^+np^+$  solar cell structure, the so-called **ALU<sup>+</sup>** cell. An independently confirmed conversion efficiency of 20% is achieved on an aperture cell area of 4 cm<sup>2</sup>, clearly demonstrating the high-efficiency potential of our **ALU<sup>+</sup>** cell concept.

## INTRODUCTION

For solar cells where  $n$ -type Czochralski-grown (CZ) silicon bulk material is used, a  $p^+$ -emitter is needed for the formation of the  $pn$ -junction. This  $p^+$ -region can e.g. be formed by a high-temperature boron-diffusion or simple a screen-printing process, where Al-paste is screen-printed on the Si wafer and subsequently fired in a conveyor belt furnace, resulting in an Al- $p^+$  emitter. The high-temperature  $p^+$  boron-diffusion has in the past mainly been used for the fabrication of high-efficiency laboratory solar cells, because it is technologically more demanding and tends to induce crystallographic defects in the bulk material degrading its recombination lifetime [1,2]. On the other hand, there is a simple screen-printing-based process for the formation of the  $p^+$ -region which is mainly used for the formation of back surface fields (BSFs) on industrial  $p$ -type crystalline silicon solar cells [3,4] and as Al- $p^+$  rear emitter on  $n$ -type crystalline silicon solar cells [5]. However, the full-area metallization of the screen-printed Al- $p^+$  emitter causes a relatively high emitter surface recombination velocity which limits the solar cell conversion efficiency. To overcome this limiting factor our **ALU<sup>+</sup>**  $n$ -type silicon solar cell concept is based on a surface-passivated screen-printed Al- $p^+$  emitter [6].

## PASSIVATED Al- $p^+$ EMITTERS

In this contribution, we determine the emitter saturation current density  $J_{0e}$  of passivated aluminum-doped  $p^+$  emitters.

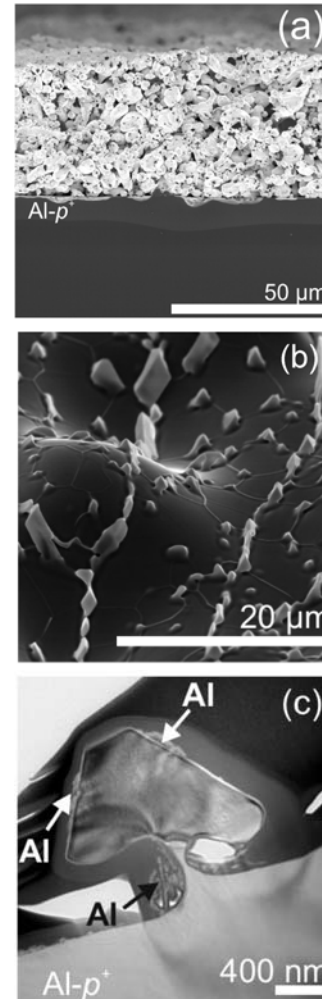


Fig. 1. (a) SEM micrograph of a cross section of a screen-printed Al- $p^+$  emitter. The Al- $p^+$  region is clearly visible as brighter contrast beneath the residual Al paste [7]. (b) SEM tilted plan-view image of an Al- $p^+$  Si surface after the residual Al-paste and the Al-Si eutectic have been removed. Al-rich surface structures appear as bright contrast. (c) Cross-sectional TEM bright-field image of one individual surface structure. Positions of Al-rich material covered by a thin Si layer are marked with arrows [8].

For this purpose we fabricate asymmetric test structures using single-crystalline shiny-etched (100)-oriented 300  $\mu$ m thick  $p$ -type float-zone (FZ) silicon wafers of 200  $\Omega$ cm resistivity, where first one side of the wafer is passivated with PECVD-SiN<sub>x</sub> and second, on the other wafer surface, the  $p^+$ -emitter is prepared by applying a conventional screen-printing process. Subsequently, the samples undergo a firing process in an infrared conveyor belt furnace at 900°C for 13 s. In

order to passivate the Al- $p^+$  emitter surface, the residues of the aluminum paste and the aluminum-silicon eutectic are removed from the Al- $p^+$  region in an HCl solution.

Figure 1(a) shows a cross-sectional scanning electron microscopy (SEM) image of a screen-printed Al- $p^+$  sample obtained from an ultra-high resolution Hitachi S-4800 field emission SEM. The Al-doped  $p^+$ -region appears brighter than the high-resistivity bulk of the silicon wafer due to the potential contrast [9]. From this picture we determine the Al- $p^+$  depth to be  $8 \pm 1 \mu\text{m}$ . Figure 1(b) shows a tilted plan view SEM image of the Al- $p^+$  surface after the residual Al paste and the Al-Si eutectic have been removed in boiling 37% HCl solution. Surface islands appear as bright contrast on top of the dark Al- $p^+$  surface. The typical lateral dimension of the islands is in the range between 1 and 3  $\mu\text{m}$ . Figure 1(c) shows a cross-sectional TEM bright field image of an island, prepared by the focused ion beam method. From this image no defects such as dislocations or grain boundaries or other crystallographic defects can be found within the bulk of the island. The island is completely defect-free and of the same crystallographic orientation as the Al- $p^+$  bulk and thus epitaxially grown. An EDX elemental mapping as well as detailed EDX line scans (not shown here) of the surface island as depicted in Fig. 1 (c) show an increased Al signal below a Si signal at the arrow marked positions of the island. This finding leads to the conclusion that Al-rich material is covered by a thin Si layer at these positions [8].

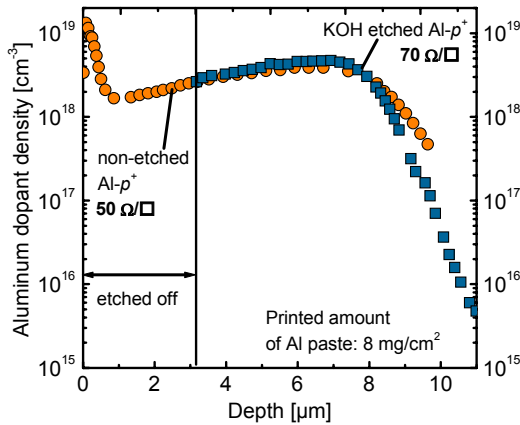


Fig. 2. Doping profiles of the same screen-printed Al- $p^+$  sample. Comparison of the doping profile before and after KOH etching step, measured by the ECV method. During the etching, the Al-rich structures are removed from the surface. The doping profile after etching shows no concentration peak at the surface.

Figure 2 shows the measured doping profile of the Al- $p^+$  region obtained by the electrochemical capacitance voltage (ECV) profiling technique with the aid of a WEP CVP21 ECV profiler. The doping profile of the screen-printed Al- $p^+$  region shows a pronounced peak close to the surface that originates from residual aluminum-rich islands on the surface which are covered by a thin Si-layer and thus are not effectively removed during the HCl etching of the Al-paste and the Al-Si eutectic [8, 10]. The islands and thus the concentration peak is removed in a KOH solution at 70°C. In this etching step, 3  $\mu\text{m}$  of the  $8 \pm 1 \mu\text{m}$  thick Al- $p^+$  region are

removed, which is demonstrated in Fig. 2 by ECV measurements taken before and after KOH etching. The emitter thickness after KOH etching was additionally determined from SEM micrographs (not shown here) at different sample positions to be  $5 \pm 1 \mu\text{m}$ , indicating that the Al- $p^+$  emitter is completely closed after etching. The sheet resistance is determined from four-point-probe measurements to be  $50 \Omega/\square$  for the 8  $\mu\text{m}$  deep emitter and to be  $70 \Omega/\square$  for the 5  $\mu\text{m}$  deep Al- $p^+$  emitter.

After the removal of the concentration peak we use single-layer PECVD a-Si and ALD- $\text{Al}_2\text{O}_3$  as well as  $\text{Al}_2\text{O}_3/\text{SiN}_x$  stacks to passivate our samples. We deposit a 20 nm thick PECVD a-Si layer at 225°C in a Plasmalab 80 PECVD reactor from Oxford Instruments. The 30 nm ALD- $\text{Al}_2\text{O}_3$  films are deposited by alternating  $\text{Al}(\text{CH}_3)_3$  dosing and  $\text{O}_2$  plasma exposure in a remote-plasma ALD-reactor (Oxford Instruments FlexAL™) at a substrate temperature of 200°C [11]. From 255 cycles of 4 s each we obtain 30 nm thick  $\text{Al}_2\text{O}_3$  films as determined by *in situ* spectroscopic ellipsometry. Subsequently, the samples received a 30 min annealing at 425°C in  $\text{N}_2$  atmosphere.

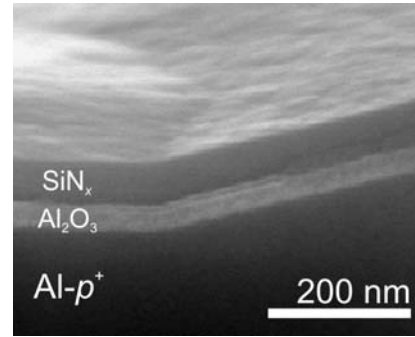


Fig. 3. Tilted cross-sectional SEM image of an Al- $p^+$  emitter passivated by an  $\text{Al}_2\text{O}_3/\text{SiN}_x$  stack.

The  $\text{Al}_2\text{O}_3/\text{SiN}_x$  stack was prepared using a 60 nm thick PECVD- $\text{SiN}_x$  capping layer with a refractive index  $n = 2.1$  deposited at 400°C on top of the 30 nm thick  $\text{Al}_2\text{O}_3$  layer.

Figure 3 shows a tilted cross-sectional SEM image of an Al- $p^+$  emitter passivated by an  $\text{Al}_2\text{O}_3/\text{SiN}_x$  stack where the  $\text{Al}_2\text{O}_3$  layer appears as bright contrast in-between the Al- $p^+$  emitter beneath and the PECVD- $\text{SiN}_x$  capping layer on top of it.

The emitter saturation current densities  $J_{0e}$  are measured before and after firing in a conveyor belt furnace at 900°C for 13 s. Emitter saturation current densities  $J_{0e}$  are obtained from transient photoconductance decay (PCD) carrier lifetime measurements using a WCT-100 lifetime tester from Sinton Consulting according to the following equation [12]:

$$\frac{1}{\tau_{\text{eff}}} = \frac{1}{\tau_{\text{bulk}}} + \frac{S_{\text{SiN}_x}}{W} + \frac{J_{0e} \Delta n}{qn_i^2 W}, \quad (1)$$

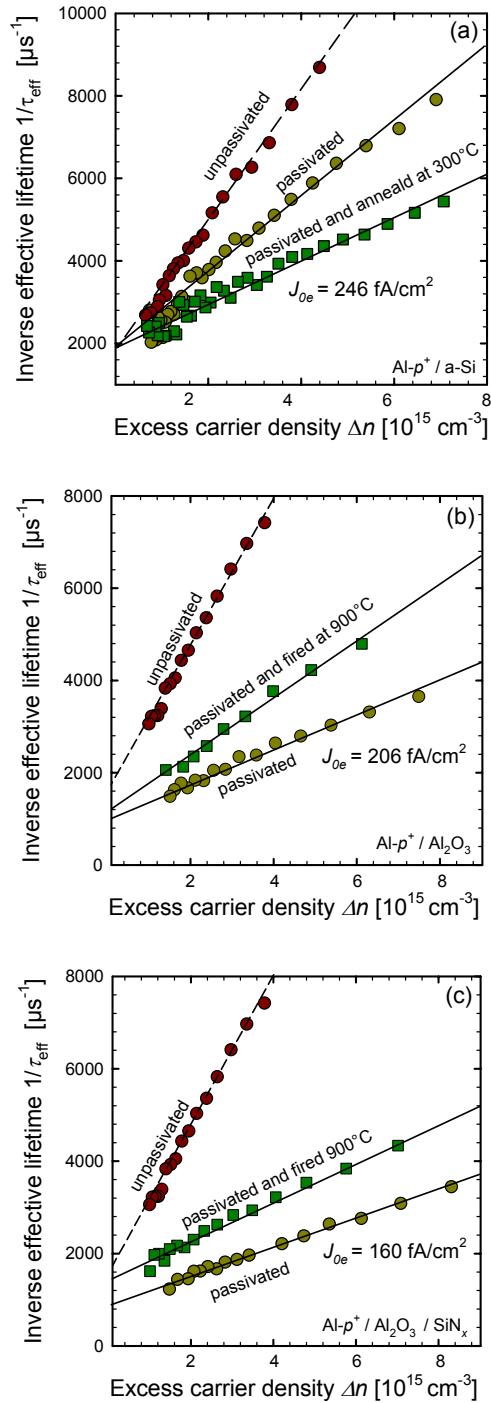


Fig. 4. Measured inverse effective lifetime  $1/\tau_{\text{eff}}$  as a function of the excess carrier density  $\Delta n$ . The substrate is a 200  $\Omega\text{cm}$  FZ Si wafer of 300  $\mu\text{m}$  thickness. The  $\text{Al-}p^+$  region covers only one side of the wafer, the other surface is well passivated by  $\text{SiN}_x$ . (a) a-Si-passivated [7], (b)  $\text{Al}_2\text{O}_3$ -passivated, and (c)  $\text{Al}_2\text{O}_3/\text{SiN}_x$ -passivated  $\text{Al-}p^+$ .

where  $W$  is the wafer thickness and  $n_i = 1 \times 10^{10} \text{ cm}^{-3}$  is the intrinsic carrier concentration of silicon at 300 K. It is assumed that the excess carrier concentration  $\Delta n$  is uniform throughout the base, which is not strictly valid for large surface recombination velocities. Due to the given asymmetry between the front and the rear side of

the sample the emitter saturation current density tends to be underestimated up to 10% for the worst-case scenario [13]. Due to the high substrate resistivity of 200  $\Omega\text{cm}$ , all lifetime measurements in this study are performed under high-injection conditions.

Figures 4 (a-c) show the measured inverse effective lifetime  $1/\tau_{\text{eff}}$  as a function of the injection density  $\Delta n$  measured on the a-Si-, the  $\text{Al}_2\text{O}_3$ -, and  $\text{Al}_2\text{O}_3/\text{SiN}_x$ -passivated samples. We measure a  $J_{0e}$  of  $800 \pm 200 \text{ fA/cm}^2$  for an unpassivated  $\text{Al-}p^+$  emitter. After the emitter surface has been passivated by an a-Si film [Fig. 4 (a)] the  $J_{0e}$  decreases to  $490 \pm 120 \text{ fA/cm}^2$ . Annealing at 300°C for 10 min further reduces  $J_{0e}$  to  $246 \pm 60 \text{ fA/cm}^2$  [7]. The  $\text{Al}_2\text{O}_3$ -passivated  $\text{Al-}p^+$  emitter [Fig. 4 (b)] exhibits a  $J_{0e}$  of  $206 \pm 40 \text{ fA/cm}^2$  and a  $J_{0e}$  of  $265 \pm 50 \text{ fA/cm}^2$  after the sample has been fired at 900°C for 13 s. On the samples passivated by  $\text{Al}_2\text{O}_3/\text{SiN}_x$  double layers [Fig. 4 (c)] we measure  $J_{0e}$  values as low as  $160 \pm 120 \text{ fA/cm}^2$  (corresponding to a  $V_{\text{OC}}$  limit of 682 mV), which is the lowest  $J_{0e}$  value reported so far for screen-printed  $\text{Al-}p^+$  region on silicon. A still remarkably low  $J_{0e}$  of  $228 \pm 45 \text{ fA/cm}^2$  (corresponding to a  $V_{\text{OC}}$  limit of 672 mV) is measured after a high-temperature firing step has been applied to the sample passivated by the  $\text{Al}_2\text{O}_3/\text{SiN}_x$  double layer, which enables an industrial application of the  $\text{Al}_2\text{O}_3/\text{SiN}_x$  double layer due to its excellent stability under firing conditions.

## THE ALU<sup>+</sup> CELL CONCEPT

Figure 5 shows two possible realizations of an **ALU<sup>+</sup>** cell with surface-passivated screen-printed  $\text{Al-}p^+$  rear emitter [6]. The a-Si surface passivation is applied to the rear side of the cell with a locally evaporated contact grid [Fig. 5 (a)] and a full-area metallized emitter featuring local point contact openings [Fig. 5 (b)]. As base material we use (100)-oriented phosphorus-doped Czochralski-grown silicon wafers with a thickness of  $\sim 190 \mu\text{m}$  and a resistivity of  $\sim 3 \Omega\text{cm}$ . After growing a 220 nm thick thermal oxide on both wafer surfaces,  $2 \times 2 \text{ cm}^2$  diffusion windows are opened on the front by means of photolithography and random pyramids are formed within the opened windows using a KOH/isopropanol solution. Afterwards, we perform a phosphorus diffusion in the diffusion windows at the front, resulting in an  $n^+$  region, which subsequently undergoes a wet oxidation. Two different FSF-diffusions have been applied to the cells resulting in a sheet resistance of 40  $\Omega/\square$  and 100  $\Omega/\square$ , respectively. After the wet oxidation at 850°C we finally obtain sheet resistances of 120  $\Omega/\square$  and 250  $\Omega/\square$ , respectively. During this oxidation the phosphorus concentration peak is mostly oxidized, resulting in an  $n^+$  front surface field (FSF) with an easy-to-passivate low surface doping concentration of  $7 \times 10^{19}$  and  $3 \times 10^{19} \text{ cm}^{-3}$ , respectively. Subsequently, the remaining oxide is removed from the wafer surface by means of a short HF dip and the textured front side is covered by a 200 nm  $\text{SiN}_x$  layer to protect the front surface from etching during the later back-etching procedure of the rear emitter.

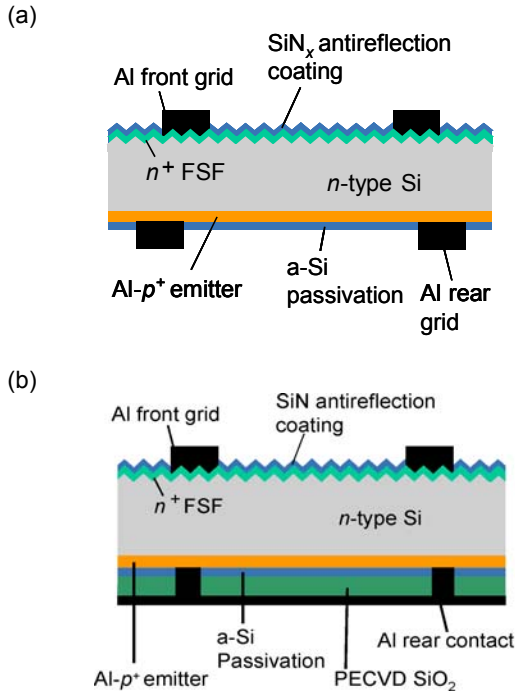


Fig. 5. Two realizations of the  $ALU^+$  cell concept featuring a screen-printed  $Al-p^+$  emitter passivated with a thin a-Si layer. (a) Evaporated Al-grid on the a-Si passivated rear emitter [6], (b) full-area metallized a-Si passivated emitter with local point contacts.

After screen-printing and firing of the  $Al-p^+$  rear emitter, the residual Al paste and the Al-Si eutectic are removed in a boiling 37% solution of HCl and the  $Al-p^+$  emitter is etched back by 2-3  $\mu m$  in a KOH solution at 70°C. The protective  $SiN_x$  coating is removed from the front side and the wafer undergoes a further wet chemical cleaning before the emitter surface is passivated by a 20 nm thick a-Si layer deposited by means of PECVD at 225°C. Then, on one cell type we evaporate rear contact grids through shadow masks with metallization fractions of ~4% (finger spacing 2 mm) and of ~6% (finger spacing 1 mm) respectively [Fig. 5 (a)]. The other cell type received a 200 nm thick PECVD- $SiO_2$  layer at the rear side where the rear contact points are opened photolithographically. After local contact opening, a full-area Al layer is evaporated on the rear side [Fig. 5 (b)]. For both cell types an Al front contact grid is evaporated through a shadow mask with a metallization fraction of ~3%. As the last process step, the  $SiN_x$  antireflection coating is deposited onto the front of all solar cells. During the  $SiN_x$  deposition at 400°C the a-Si underneath the Al contacts dissolves and the Al at the rear contacts the  $Al-p^+$  emitter [14].

## RESULTS

The one-sun performance of the processed  $ALU^+$   $n$ -type solar cells featuring the a-Si passivated  $Al-p^+$  emitter is shown in Table 1. Cells P01 and P25 feature evaporated Al-grids at the rear and an  $n^+$  FSF of 120  $\Omega/\square$  and 250  $\Omega/\square$ , respectively [Fig. 5 (a)]. Cell P15 corresponds to the full-area rear metallization and point-contact openings at the rear and an  $n^+$  FSF of 250  $\Omega/\square$  [Fig. 5 (b)].

Table 1  $ALU^+$  solar cell parameters measured under standard testing conditions (AM1.5G, 100  $mW/cm^2$ , 25°C). Cells P01 and P25 correspond to Figs. 5 (a) and Cell P15 corresponds to Fig. 5 (b). The aperture cell area is 4  $cm^2$ .

Cell ID	$V_{oc}$ [mV]	$J_{sc}$ [ $mA/cm^2$ ]	FF [%]	$\eta$ [%]
P01	649	39.1	77.5	19.7* [15]
P25	636	39.5	79.5	20.0*
P15	639	39.9	77.2	19.7*

\* independently confirmed at Fraunhofer ISE CaLab

We achieve open-circuit voltages  $V_{oc}$  up to 649 mV demonstrating the excellent emitter quality and the effective surface passivation of the  $Al-p^+$  emitter. The highest  $V_{oc}$  achieved for  $n$ -type solar cells with full-area metallized  $Al-p^+$  emitter in the past was  $V_{oc} = 627$  mV [16]. Note that more recently, a  $V_{oc}$  of 645 mV has been reported for  $n$ -type Si solar cells featuring an a-Si-passivated  $Al-p^+$  emitter using 10  $\Omega cm$   $n$ -type float-zone material [17]. The corresponding cell efficiency was 19.5%. In the literature, an ultimate  $V_{oc}$  limit of 641 mV has been estimated for full-area screen-printed  $Al-p^+$  emitters [18]. Our newly developed surface-passivated  $Al-p^+$  emitter clearly outperforms this  $V_{oc}$  limit.

The very high short-circuit current density of our cells is in the range of  $J_{sc} = 39.1 - 39.9$   $mA/cm^2$ , which confirms a very effective minority-carrier diffusion to the rear junction. For our best cell (see Table 1, cell P25) an energy conversion efficiency of 20.0% has been obtained, which was independently confirmed at Fraunhofer ISE CaLab, Freiburg, Germany. This is the highest efficiency attained so far for  $n$ -type Cz silicon solar cells featuring an a-Si passivated screen-printed  $Al-p^+$  emitter. The solar cell with local contact openings and a full-area metallization at the emitter surface reaches an independently confirmed cell efficiency of 19.7 % (see Table 1, cell P15) and a very high short circuit current density of 39.9  $mA/cm^2$ , which is due to the increased reflection at the rear of the cell.

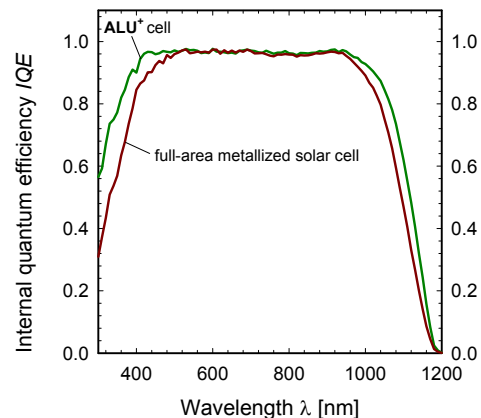


Fig. 6. Comparison of the internal quantum efficiency of a "standard"  $n$ -type solar cell with a fully metallized screen-printed rear  $Al-p^+$  emitter and an  $ALU^+$  solar cell with an a-Si-passivated screen-printed  $Al-p^+$  rear emitter.

Figure 6 shows the internal quantum efficiency (*IQE*) calculated from the external quantum efficiency measured at 1/3 sun bias light intensity and the measured reflectance data of a standard *n*-type solar cell with a fully metallized Al-*p*<sup>+</sup> rear emitter and in comparison the *IQE* of an **ALU**<sup>+</sup> solar cell featuring an a-Si passivated Al-*p*<sup>+</sup> emitter and an optimized front side. High *IQE* values above 0.95 are achieved at  $\lambda = 500 - 900$  nm for both solar cells. The **ALU**<sup>+</sup> cell shows an increased *IQE* at  $\lambda > 950$  nm due to the a-Si passivated Al-*p*<sup>+</sup> emitter surface. Also a significantly higher *IQE* is obtained for the **ALU**<sup>+</sup> cell at  $\lambda < 500$  nm which can be explained by lower surface recombination at the front side due to the 250  $\Omega/\square$  *n*<sup>+</sup> FSF with an easy-to-passivate low surface doping concentration of  $3 \times 10^{19}$  cm<sup>-3</sup> [19].

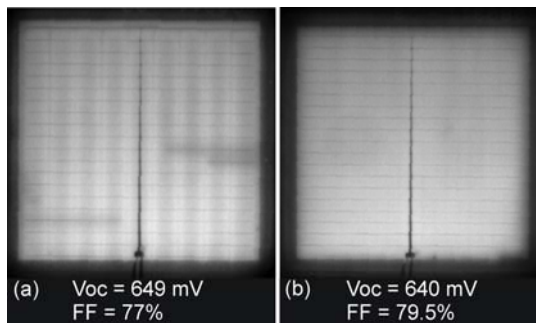


Fig. 7. (a) Electroluminescence (EL) image at an applied voltage  $V_{appl.}$  of 646 mV of an **ALU**<sup>+</sup> solar cell with a non-optimized metallization grid on the rear showing a decreased EL signal between the metallization fingers due to series resistance problems. (b) Electroluminescence image at an applied voltage  $V_{appl.}$  of 644 mV of a solar cell with an optimized metallization grid at the rear side showing a homogeneous EL signal.

Figure 7 (a) shows an electroluminescence (EL) image at an applied voltage  $V_{appl.}$  of 646 mV of a **ALU**<sup>+</sup> solar cell with a non-optimized metallization grid at the Al-*p*<sup>+</sup> emitter surface with a finger spacing of 2 mm (corresponding cell P01 from Table 1). The large fraction of well-passivated emitter surface results in a high  $V_{oc}$  of 649 mV, whereas the EL-signal drops significantly between the fingers due to a high series resistance. This results in a low fill factor *FF* of 77%. In comparison to that, Fig. 7 (b) shows an electroluminescence image at an applied voltage  $V_{appl.}$  of 644 mV of a solar cell with an optimized metallization grid at the Al-*p*<sup>+</sup> emitter surface with a finger spacing of 1 mm (corresponding to cell P25 from Table 1). A homogenous EL signal throughout the cell area can be observed. Due to the higher fraction of metallized emitter surface and thus increased recombination, a reduced  $V_{oc}$  of 640 mV is obtained. The optimized contact-grid geometry results, however, in an increased fill-factor *FF* of 79.5% and a record-high efficiency of  $\eta=20.0\%$ .

## CONCLUSIONS

Using carrier lifetime measurements we have shown that screen-printed Al-*p*<sup>+</sup> emitters can be effectively passivated by thin layers of amorphous silicon deposited

by PECVD as well as by atomic-layer-deposited aluminum oxide. Al<sub>2</sub>O<sub>3</sub>/SiN<sub>x</sub> stacks led to the lowest emitter saturation current densities of  $J_{0e} = 160$  fA/cm<sup>2</sup> achieved so far on screen-printed Al-*p*<sup>+</sup> emitters. Even more important is the finding that the passivation quality of Al<sub>2</sub>O<sub>3</sub> films as well as Al<sub>2</sub>O<sub>3</sub>/SiN<sub>x</sub> stacks show an excellent stability during firing at 900°C.

We have demonstrated the high potential of *n*<sup>+</sup>*np*<sup>+</sup> **ALU**<sup>+</sup> solar cells by implementing an a-Si passivation to a screen-printed aluminum-alloyed rear *p*<sup>+</sup> emitter. For our best cell an independently confirmed efficiency of 20.0 % is obtained on *n*-type Czochralski-grown silicon material. This is the highest efficiency reported so far for an *n*-type Cz-Si solar cell featuring an easy-to-fabricate screen-printed a-Si-passivated rear-side Al-*p*<sup>+</sup> emitter. Our results suggest that the efficiency potential of screen-printed solar cells on *n*-type silicon has been strongly underestimated in the past.

## Acknowledgments

Funding was provided by the State of Lower Saxony and the German Ministry for the Environment, Nature Conservation and Nuclear Safety (BMU) under Contract No. 0327666.

## REFERENCES

- [1] J. Zhao and A. Wang, Proceedings of the 4th World Conference on Photovoltaic Energy Conversion, Hawaii, USA (IEEE, New York, 2006) p. 996.
- [2] P. J. Cousins and J. E. Cotter, *Proceedings of the 31st IEEE Photovoltaic Specialists Conference*, Orlando, USA (IEEE, New York, 2005), p. 1047.
- [3] G. C. Cheek, R. P. Mertens, R. Van Overstraeten, and L. Frisson, *IEEE Trans. Electron Devices*, ED-31, 602 (1964).
- [4] C.F. Gay, in *Proceedings of the 13th IEEE Photovoltaic Specialists Conference*, p. 444, IEEE (1978).
- [5] A. Cuevas, C. Samundsett, M. J. Kerr, D. H. Macdonald, H. Mäckel, and P. Altermatt, *Proceedings of the 3rd World Conference on Photovoltaic Energy Conversion*, Osaka, Japan (2003), p. 963.
- [6] Patent pending, ISFH
- [7] R. Bock, J. Schmidt, and R. Brendel, *Appl. Phys. Lett.* **91**, 112112 (2007).
- [8] R. Bock, J. Schmidt, R. Brendel, H. Schuhmann, and M. Seibt, *J. Appl. Phys.* **104**, 043701 (2008.)
- [9] Cordelia P. Sealy, Martin R. Castell, and Peter R. Wilshaw, *Journal of Electron Microscopy* **49**, 311-321 (2000).
- [10] P. Lölgen and C. Leguijt, *Proceedings of the 23th IEEE Photovoltaic Specialists Conference*, Louisville, USA, (IEEE, New York, 1993), p. 236.
- [11] L. van Hemmen, S. B. S. Heil, J. Klootwijk, F. Roozeboom, C.J. Hodson, M. C. M. van de Sanden, and W. M. M. Kessels, *J. Electrochem. Soc.* **154**, G165 (2007).
- [12] R.A. Sinton and A. Cuevas, *Appl. Phys. Lett.* **69**, 2510-2512 (1996).

- [13] D.E. Kane and R.M. Swanson, *Proceedings of the 18th IEEE Photovoltaic Specialists Conference*, Las Vegas, USA, (IEEE, New York, 1985), p. 578.
- [14] H. Plagwitz, M. Nerding, N. Ott, H.P. Strunk, and R. Brendel, *Prog. In Photovolt.: Research and Applications* **12**, 47 (2004).
- [15] R. Bock, J. Schmidt, and R. Brendel, *Phys. Stat. Sol. (RRL)* **2**, No. 6, 248-250 (2008)
- [16] C. Schmiga, H. Nagel, and J. Schmidt, *Prog. Photovolt.* **14**, 533-539 (2006).
- [17] C. Schmiga, M. Hermle, and Stefan Glunz, *Proceedings of the 23rd European Photovoltaic Solar Energy Conference*, Valencia, Spain (WIP, Munich, 2008), p. 982.
- [18] A. Cuevas, C. Samundsett, M. J. Kerr, D. H. Macdonald, H. Mäkel, and P. Altermatt, *Proceedings of the 3rd World Conference on Photovoltaic Energy Conversion*, Osaka, Japan (2003), p. 963.
- [19] J. Schmidt, J.D. Moschner, J. Henze, S. Dauwe and R. Hezel, *Proceedings of the 19th European Photovoltaic Solar Energy Conference*, Paris, France (WIP, Munich, 2004), p. 391.